II

Randelhoff, A., A. Sundfjord, and M. Reigstad (2015), Seasonal variability and fluxes of nitrate in the surface waters over the Arctic shelf slope, *Geophysical Research Letters*, *42*, 3442–3449, doi:10.1002/2015gl063655.

AGU PUBLICATIONS

Geophysical Research Letters

RESEARCH LETTER

10.1002/2015GL063655

Key Points:
- First year-round moored observations of nitrate in the Eastern Arctic Ocean
- Vertical nitrate fluxes are supported by weakened stratification in fall
- Nitrate near depletion indicates nutrient limitation of annual new production

Correspondence to:
A. Randelhoff,
achim@npolar.no

Citation:
Randelhoff, A., A. Sundfjord, and M. Reigstad (2015), Seasonal variability and fluxes of nitrate in the surface waters over the Arctic shelf slope, *Geophys. Res. Lett.*, *42*, doi:10.1002/2015GL063655.

Received 6 MAR 2015
Accepted 7 APR 2015
Accepted article online 14 APR 2015

Seasonal variability and fluxes of nitrate in the surface waters over the Arctic shelf slope

Achim Randelhoff[1,2], Arild Sundfjord[2], and Marit Reigstad[1]

[1] Institute for Arctic and Marine Biology, University of Tromsø, Tromsø, Norway, [2] Norwegian Polar Institute, Tromsø, Norway

Abstract Understanding the present state and possible future scenarios of Arctic Ocean primary productivity has been hampered by the scarcity of year-round nutrient measurements. Here the first yearlong moored time series of near-surface nitrate concentrations in the Eastern Arctic, together with hydrography, currents, and chlorophyll *a* fluorescence, is reported from the shelf slope northeast of Svalbard. Variability was dominated by the inflow of Atlantic Water (AW). Nitrate was near depleted during July–September and reached a maximum concentration of 10 μM in March. Vertical nitrate gradients were eroded by mid-December, demonstrating the importance of the AW in breaking down upper ocean stratification during fall. Upward nitrate fluxes through the nitracline in the AW inflow region during fall were 2.5 ± 0.5 mmol m^{-2} d^{-1}. The spring bloom triggered extensive nitrate drawdown from June, from which an annual new production of 31 g C m^{-2} was estimated.

1. Introduction

The Arctic Ocean (AO) primary production (PP) is subject to two major constraints: Light limitation resulting both from the thick, perennial ice cover and the total absence of sunlight during the polar night and nutrient limitation by nitrate depletion due to the strong stratification in large parts of the deep basins and the Western Arctic [*Codispoti et al.*, 2013]. With the currently retreating ice cover [e.g., *Comiso*, 2012], primary production could be expected to increase as more light becomes available [*Arrigo et al.*, 2008; *Arrigo and van Dijken*, 2011]. However, the associated changes in stratification and thus upward mixing of nutrients are not well understood, such that the reliability of large-scale modeling of future AO PP largely depends on current constraints of nitrate concentrations in the ice-covered areas [*Vancoppenolle et al.*, 2013].

Since river runoff draining into the AO contains little nutrients [*Codispoti et al.*, 2013], the inflows of Atlantic Water (AW) via Fram Strait and the Barents Sea and of Pacific Water via Bering Strait are the dominant sources of nutrients for the AO [*Torres-Valdés et al.*, 2013; *Codispoti et al.*, 2013]. Because of its high salinity and successive cooling, the AW that enters the AO sinks down to intermediate depths, from where it provides nutrients to the surface waters through turbulent diapycnal mixing.

Without light limitation, the spring bloom rapidly depletes the nitrate pool in the euphotic zone, and nitrate concentrations ($\mathcal{N}$) remain low throughout summer by a combination of continued nitrate consumption and suppression of vertical mixing caused by the developing stratification [e.g., *Carmack et al.*, 2006]. In this respect, two quantities are of interest, dominated by the physical setting rather than the biological fluxes: The vertical flux of nitrate that supplies the productive surface layer during summer and the replenishment of the nitrate pool during fall and winter, which in turn determines the prebloom state for the next season. However, few observations of vertical nutrient fluxes exist in the AO [*Bourgault et al.*, 2011]. During fall, primary production ceases, stratification weakens, and surface nutrient concentrations start to increase again, and more so on the shelf [e.g., *Aagaard and Carmack*, 1994] than in the central AO. The upper part of the continental slope is an interesting region at the boundary between the deep basin and the shelf seas, with possibly elevated mixing from strong boundary current shear and possible upwelling during ice-free conditions [*Carmack and Chapman*, 2003].

Data on nutrient concentrations in the AO are sparse not only due to ice restricting access to the region but also the need for time-consuming wet chemistry to analyze water samples, which limits temporal and spatial coverage. In situ ultraviolet spectrophotometry is a tool for real-time, in situ measurements of nitrate [*Johnson and Coletti*, 2002] which allows for continuous and autonomous long-term deployments

[e.g., *Johnson et al.*, 2006]. This facilitates monitoring of $\mathcal{N}$ even in remote areas, but to our knowledge, this is the first such data set reported from the Eastern AO.

Starting in 2012, a project monitoring the AW boundary current north of Svalbard has been collecting data from a line of instrumented moorings and annual cruises. Using data from this program (A-TWAIN: Long-term variability and trends in the Atlantic Water inflow region), the present study aims to give insight into the seasonal nitrate cycle in the surface waters and the interaction between the AW inflow and the local Arctic water masses by analysis of mooring data from the upper slope north of Svalbard.

2. Methods

2.1. Data

We present a yearlong data record from a mooring deployed between September 2012 and September 2013 at 81°30′N, 30°51′E, on the shelf slope north of Svalbard over a water depth of approximately 800 m, supplemented by data from hydrographical stations made during the mooring turnaround cruises.

Two SBE16plus V2 (SeaCAT) units were moored at approximately 20 and 40 m depth, sampling temperature T, salinity S (in the following, given on the practical salinity scale), chlorophyll *a* fluorescence (chl *a*), and pressure P 4 times per hour. SBE16plus data were processed using precruise calibration coefficients provided by Seabird. A Satlantic In Situ Ultraviolet Spectrophotometer V3 nitrate sonde (ISUS) was moored approximately 1 m below the upper SeaCAT, sampling absorption between 170 and 400 nm in a 1 cm cuvette with a sampling "burst" of 13 light and 2 dark frames every 2 h.

An up-looking RD Instruments Sentinel 300 kHz acoustic Doppler current profiler (ADCP) was mounted at approximately 90 m depth. In September 2012 and 2013, conductivity-temperature-depth (CTD) casts were taken at the mooring location, along with water samples across the water column to determine nutrient and chl *a* concentrations.

2.2. ISUS Processing and Nitrate Bottle Samples

ISUS data processing followed *Sakamoto et al.* [2009], using their temperature compensated, salinity subtracted algorithm and a wave band of 217–240 nm. In situ temperature and salinity were taken as measured by the SeaCAT mounted 1 m above the ISUS. Low detector intensities close to the dark currents during parts of June, July, and August (presumably due to very turbid waters) rendered the spectral fitting method useless, thus preventing calculation of nitrate values for those periods. In addition, the ISUS did not sample during a 3 week period in March 2013 for unknown reasons. A data point was discarded if its standard deviation (based on 13 samples for each burst) exceeded 0.2 μM, which was coincident with low detector intensities. That part of the nitrate data which was not discarded had an average standard deviation of 0.12 μM, and the minimum detectable concentration difference is therefore approximately 0.5 μM (three standard deviations [*Johnson and Coletti*, 2002]).

The nitrate bottle samples were processed using a Flow Solution IV analyzer by O.I. Analytical, USA. The analyzer was calibrated using reference seawater from Ocean Scientific International Ltd., UK, and the detection limit is 0.02 μM.

Comparing bottle samples taken during the turnover cruises with ISUS values is difficult due to large vertical $\mathcal{N}$ gradients during September, and some temporal variation around the time points in question. From 15 profiling deployments of the same instrument in January 2014 (unpublished data), we infer a mean additive correction of 2 μM, the ISUS being biased high. This is consistent with bottle samples taken during the turnover cruises, but we acknowledge an overall uncertainty of approximately 1 μM in $\mathcal{N}$. Note that this introduces a large relative uncertainty at small $\mathcal{N}$, and one has to be careful about interpreting values $\mathcal{N} < 1$ μM.

Note that the bottle sample analysis yields values for the sum of nitrate and nitrite concentrations, but levels of nitrite in the AO are generally much lower than that of nitrate [e.g., *Codispoti et al.*, 2005]. We therefore refer to both nitrate concentrations measured by the ISUS and nitrate plus nitrite concentrations measured in bottle samples as nitrate concentration ($\mathcal{N}$).

2.3. Chlorophyll *a*

Analysis of chl *a* samples from the vertical profiles followed standard procedures based on *Holm-Hansen and Riemann* [1978] as described by *Reigstad et al.* [2008]. The samples were frozen on board after filtration, until analysis <4 weeks after sampling. No calibration of the chl *a* fluorescence sensors mounted on

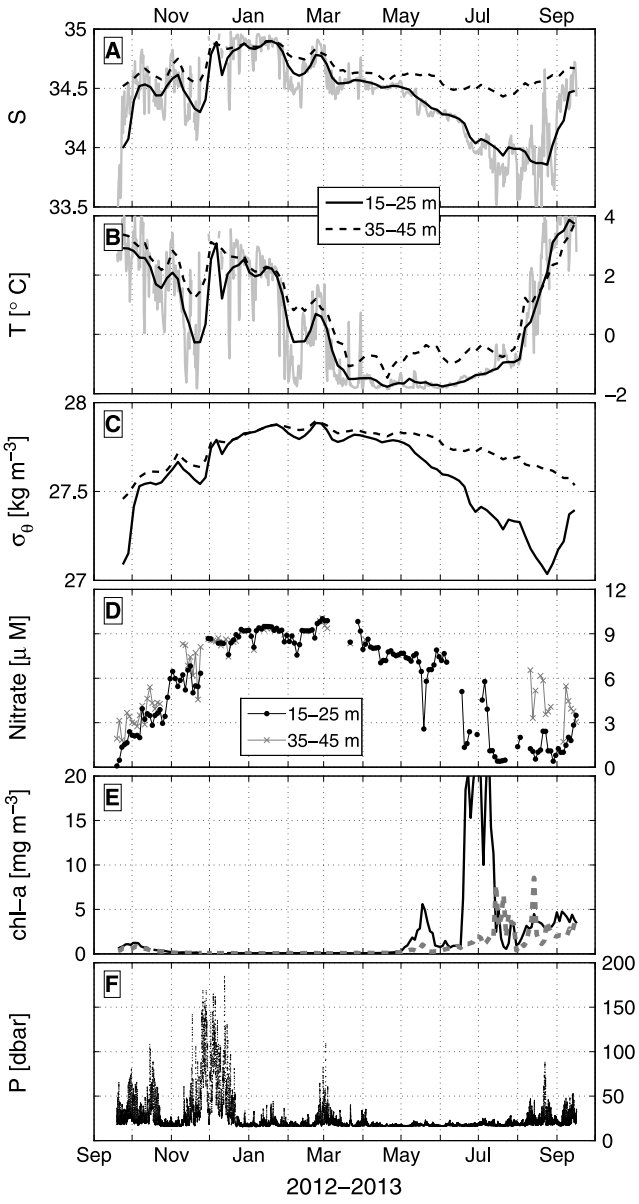

Figure 1. ISUS and SeaCAT data time series. To account for vertical motion of the mooring, only data from the indicated depth intervals are plotted (excluding Figure 1f). (a, b) Salinity and temperature between 15 and 25 (grey: 12 h mean, black solid: running 15 day mean) and 35 and 45 m (broken, running 15 day mean). (c) σ_θ (running 15 day mean) between 15 and 25 (solid) and 35 and 45 m (broken line). (d) Nitrate, 15–25 m (black, dots) and 35–45 m (grey, crosses). (e) Chl *a* fluorescence at 15–25 (solid black) and 35–45 m (broken, grey). (f) Pressure at the upper SeaCAT, mounted 1 m above ISUS.

the moored SeaCATs was done. The values plotted in Figure 1e therefore have to be regarded as qualitative values.

2.4. Vertical Profiles

The moored instruments underwent considerable dive-and-rise cycles during the deployment period, most notably in November and December 2012, as measured by the SeaCATs' pressure sensors (Figure 1f). These dives and climbs frequently happened in the course of less than 24 h, enabling us to infer approximate vertical profiles of the upper ~150–200 m. The overall coverage is patchy, but good enough during fall 2012 to infer monthly averages. Potential density (σ_θ) and $\mathcal{N}$ data were sorted into 18 depth bins of 10 m depth between 15 and 195 m and further averaged in 30 day intervals to account for the large variability on time scales of days to weeks. Although some density profiles show negative gradients (Figure 3e), this is rather an artifact of temporal variability, resolved differently at different depths, than actual unstable stratification. Overall results were not sensitive to the exact averaging method, and the profiles could not be improved consistently by more elaborate methods.

2.5. Ice and Wind Conditions

Advanced Microwave Scanning Radiometer 2 (AMSR-2) data (September 2012 to October 2013) were downloaded from http://www.iup.uni-bremen.de:8084/amsr2data/asi_daygrid_swath/n3125/ on 8 April 2014. Ice concentrations were gridded on a stereographic projection centered at the mooring location and averaged inside a radius of 20 km around the mooring location. Wind velocity from the nearest grid point (81.75°N, 30.75°E) was taken from the ERA-Interim global reanalysis [*Dee et al.*, 2011], downloaded from http://apps.ecmwf.int/datasets/data/interim_full_daily/ on 28 August 2014.

3. Results

3.1. Seasonal Cycle

T, *S*, and $\mathcal{N}$ exhibited a clear cycle through the 1 year data record (Figure 1). While *S* had a clear seasonal maximum roughly in December–January and a minimum in July–August 2013 (Figure 1), the temperature minimum was spread over April–July 2013, and there was no isolated maximum but rather two peaks, one in

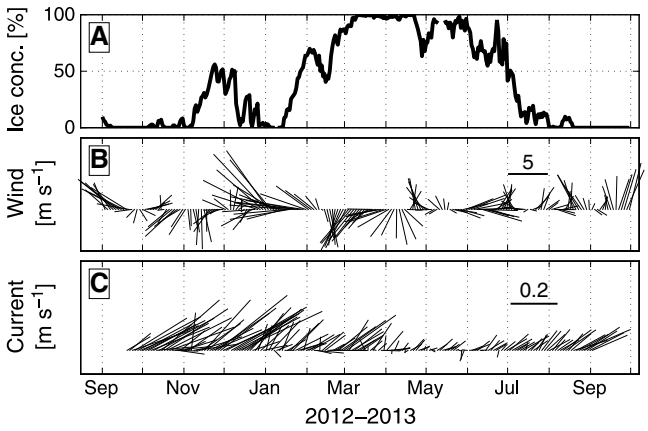

Figure 2. (a) Average ice concentration in a radius of 20 km around the mooring location (from AMSR-2). The radius was chosen arbitrarily, and the mean concentration is not sensitive to its exact value. (b) Ten meter wind (15 day running mean) at 81.75°N, 30.75°E from ERA-Interim. (C) The 15–25 m averaged current (2 day mean) from upward looking ADCP, with north up and east right.

September and one in December 2012, separated by a ~3°C cooling and warming in between. Variation in T and S on timescales of days to weeks was much larger in winter than in summer. Nitrate was at its maximum winter concentration between January and March (Figure 1) with a maximum of 10 μM in March, and it was near depleted in the summer months July and August, with the largest drawdown starting in June.

Although wind direction varied considerably, water currents at 15–25 m followed the shelf slope eastward at maximum speeds of roughly 0.4 m s^{-1}, and with little influence of the wind stress on the overall flow direction (Figure 2).

3.2. Hydrographical Profiles

At the hydrographical stations during the cruises both in 2012 and 2013, the September mixed layer was about 25 m deep, with temperatures of about 2.4°C (Figure 3). The bottle sample profile from September 2012 (Figure 3) showed a nutrient-depleted surface layer of about 20 m depth, overlying a nitracline extending to roughly 100–150 m. Mixed-layer nitrate concentrations were higher (about 2 μM) in 2013, but the nitracline started at 30–50 m in both 2012 and 2013. Chl *a* fluorescence was very low in September both in 2012 and 2013, indicating that most primary production had ceased by then.

3.3. Vertical Structure and Nitrate Fluxes

From vertical profiles of nitrate (Figure 3), we infer an initially strong gradient which was eroded throughout fall. Sometime in mid-December, values reached $\mathcal{N} \approx 9$ μM and the nitrate gradient vanished where the pycnocline was located in the previous summer (25–45 m), but the nitrate concentration itself continued to rise throughout winter to approximately 10 μM. The pattern for σ_θ profiles was similar, with vanishing stratification in December. From the nitrate profiles during fall, we can calculate nitrate fluxes as follows. The conservation equation for $\mathcal{N}$ is

$$\partial_t \mathcal{N} + U\partial_x \mathcal{N} = \partial_z F_{\mathcal{N}} + Q_{\mathcal{N}} \ , \tag{1}$$

where $F_{\mathcal{N}}$ is the vertical turbulent nitrate flux, $Q_{\mathcal{N}}$ is a source term, and U is the mean horizontal (advection) velocity. Assuming no source or sink,

$$\Sigma F_{\mathcal{N}}(h) \equiv F_{\mathcal{N}}(h) - \int_0^h \mathrm{d}z U\partial_x \mathcal{N} \simeq \int_0^h \mathrm{d}z\, \partial_t \mathcal{N} \ , \tag{2}$$

where $\Sigma F_{\mathcal{N}}$ represents the total nitrate flux into the water column between depth h and the surface. In September 2012, the well-mixed layer was approximately 25 m deep (Figure 3), and the difference in σ_θ between 20 and 40 m is small from October 2012 through May 2013 (Figure 1). Therefore, we assume constant $\mathcal{N}$ from the 15–25 m depth bin and up throughout the period of September–January. Profiles of $\partial_t \mathcal{N}$ are then approximated from the profiles "Sep/Oct" through "Dec/Jan" (Figure 3) to give three independent estimates of $\Sigma F_{\mathcal{N}}$ throughout fall, the mean of which is 2.5 ± 0.5 mmol m^{-2} d^{-1} (1 standard deviation) at $h = 35$ m, which was in the uppermost part of the nitracline in September 2012. The result is not strongly sensitive to h.

4. Discussion

4.1. Hydrography

The measurements show a highly variable environment, with frequent shifts between more Atlantic (warmer, saltier) and more Arctic-influenced (colder, fresher) water masses, dominating variability on time scales shorter than a few months (Figure 4). This variability was strongest in winter, possibly associated with frequent

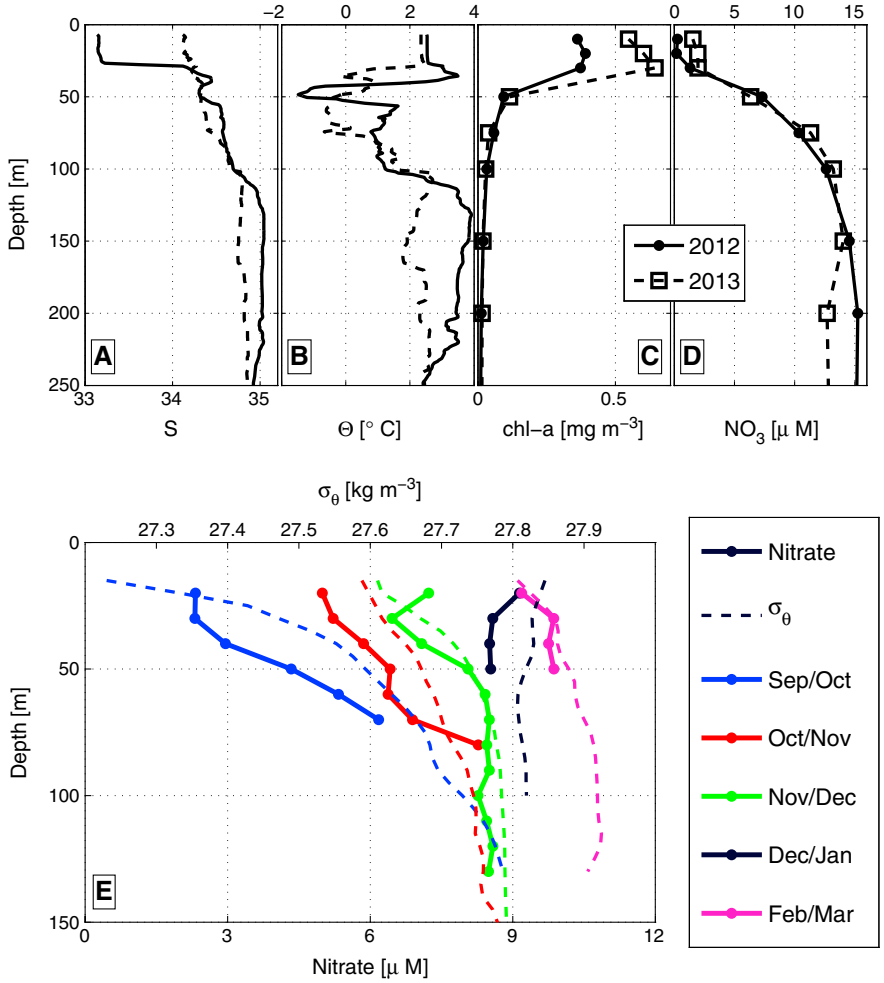

Figure 3. CTD profiles of (a) salinity, (b) potential temperature, (c) chl *a* fluorescence (from bottle samples), and (d) nitrate (from bottle samples) at the mooring location on 17 September 2012 (solid) and 16 September 2013 (dashed). (e) Vertical profiles of $\mathcal{N}$ and potential density (σ_θ), inferred from dives of the mooring.

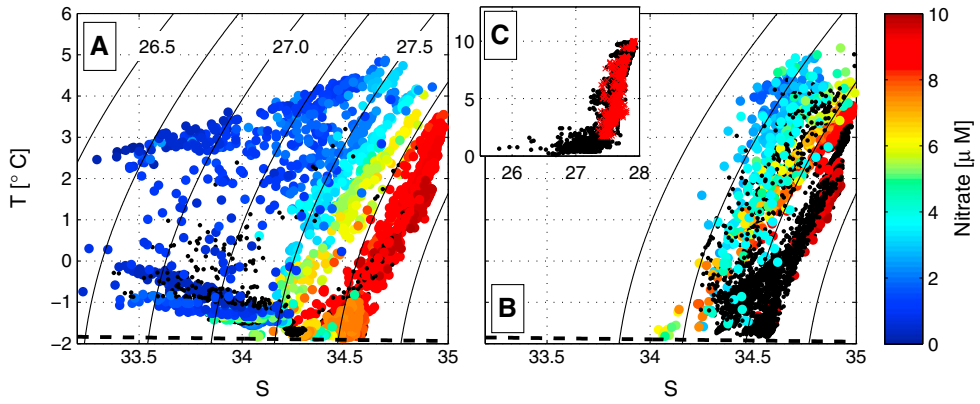

Figure 4. *T-S* plots at (a) 15–25 m and (b) 35–45 m. Nitrate concentration ($\mathcal{N}$) is color coded where available, otherwise black. The dashed line shows the seawater freezing point; isolines are σ_θ (labels in kg m^{-3}). (c) $\mathcal{N}$ (μM) (on the *y* axis) versus σ_θ (kg m^{-3}) (on the *x* axis) for 15–25 m (black dots) and 35–45 m (red crosses).

advection events of sea ice and Arctic water masses which mixed with the AW inflow. Summer was characterized by colder and fresher water, and less variability. This is reflected in the current measurements, which show much larger velocities in the October–March period than in April–July.

In the same area, *Ivanov et al.* [2009] found a significant seasonal signal in the *T-S* properties of the AW at depths ranging between 70 and 215 m, with a clear distinction between warmer/saltier and colder/fresher water types, present during winter and summer, respectively. To assess the influence of the AW variability on surface measurements, we compare density ratios $R = \alpha\Delta T/\beta\Delta S$, where α and β are the thermal expansion and haline contraction coefficients evaluated at the annual-mean T and S and the respective depths and ΔT, ΔS are the seasonal amplitudes of temperature and salinity. *Ivanov et al.* [2009] found $R = 4.2$–15.5 at depths of 70–215 m, versus far lower cooling versus freshening ratios (0.34 and 0.81 at 15–25 and 35–45 m, respectively) in our study. This indicates that the surface water variability was dominated by the freeze/melt cycle of the ice cover instead of the AW cooling/warming cycle. Even so, the weakening of the stratification through fall 2012 (Figure 3) was aided by the inflow of high-salinity near-surface AW that helped to break down salinity stratification when freshwater input from sea ice melt ceased after summer.

4.2. Nitrate Variability

The seasonal nitrate variability reflected the overall cycle of a bloom in summer, depletion or near depletion following the bloom, and replenishment during the following fall and winter. The brief low-$\mathcal{N}$-high-chl *a* event in mid-May was likely due to advection of a small patch that had been productive earlier and may or may not have been productive when it passed the mooring. The abrupt nitrate drawdown starting in June was presumably caused by the onset of primary production (Figure 1e). This is consistent with the retreat of the ice cover (Figure 2a), which allowed sunlight to enter the upper ocean and trigger the bloom, possibly in combination with strengthening stratification due to enhanced ice melt. However, nitrate drawdown was not monotonous. Instead, $\mathcal{N}$ was highly variable during the productive season, indicating horizontal patchiness, as has previously been observed in the northern Barents Sea [*Falk-Petersen et al.*, 2000].

$\mathcal{N}$ was strongly related to σ_θ, where the $\mathcal{N} - \sigma_\theta$ slopes were about the same for the intervals between 15 and 25 and 35 and 45 m ($R^2 = 0.71$ and 0.68, respectively; see Figure 4c) at $\mathcal{N} > \sim 2$ μM, below which more freshening occurred than $\mathcal{N}$ reduction. It is not clear what made this relation so tight, even though it stresses the coupling of primary producers to stratification.

4.3. Nitrate Fluxes During Fall

The nitrate flux $\Sigma F_{\mathcal{N}}$ potentially comprises four contributions: Vertical flux $F_{\mathcal{N}}$, nitrate uptake by phytoplankton, nitrification, and horizontal advection. In the following, we argue that the last three are minor during fall and thus $F_{\mathcal{N}} \approx \Sigma F_{\mathcal{N}}$. Quantifying the vertical nitrate fluxes during fall gives insight into how vertical mixing is controlled by the physical conditions developed during summer and thus constrains the postbloom supply of allochthonous nitrate to the euphotic zone.

Chl *a* fluorescence was close to zero throughout the September 2012 to January 2013 period, so nitrate uptake vanishes. *Tremblay et al.* [2008] concluded that for their data set from the coastal Beaufort Sea, nitrification accounted for 1.4 nM d^{-1}, or 11%, of the observed $\mathcal{N}$ increase after the establishment of the fast ice cover. Assuming that this rate (realistically the magnitude, but the same even holds when considering the ratio) approximately applies to our study region, nitrification accounted at most for a small part of $\Sigma F_{\mathcal{N}}$.

As stated earlier, the current regime was clearly dominated by the inflow of Atlantic Water [see, e.g., *Schauer et al.*, 2004] through the whole measurement period. This is important to note during the following discussion of advective fluxes. Advection may be split into two parts: Along slope (with the AW) and cross slope. Since $\mathcal{N}$ can be expected to evolve differently on and off the shelf, there might be a horizontal cross-slope gradient. Overall, cross-slope transport events were only episodic, since upper ocean currents during the study period were mainly eastward and along shelf (that is, following the AW; see Figure 2) especially during fall, indicating that integrated over the whole fall-winter period, advection of AW would dominate over cross-slope transport. During fall, one might speculate that farther upstream, the AW inflow is less vertically stratified, enhancing $F_{\mathcal{N}}$ and setting up a horizontal downstream gradient, thus leading to a positive contribution from advection. However, since summertime surface AW is also depleted in nitrate, the vertical $\mathcal{N}$ gradient would be similar upstream of the mooring, such that $F_{\mathcal{N}} \approx \Sigma F_{\mathcal{N}}$ when integrated over the upstream region.

To see whether $\Sigma F_{\mathcal{N}}$ is a reasonable magnitude for a vertical turbulent flux, we can also compare the eddy diffusivities K estimated from nitrate fluxes and from a theoretical dissipation scaling (see Appendix A). The results are consistent with the arguments above and indicate that $\Sigma F_{\mathcal{N}}$ is an upper bound on $F_{\mathcal{N}}$.

Bourgault et al. [2011] reported $F_{\mathcal{N}} = 0.5$ mmol m^{-2} d^{-1} from fall and winter observations in the Amundsen Gulf, that is, with 90% ice cover and in a strongly stratified water column. They also compile several observations of turbulent nitrate fluxes in various parts of the world ocean, with fluxes varying greatly between about 0.01–10 mmol m^{-2} d^{-1}. *Sundfjord et al.* [2007] reported 0.1-2 mmol m^{-2} d^{-1} for the Barents Sea (May and July, 40–90% ice cover). In general, we can expect somewhat higher fluxes due to persistently high wind speeds during fall/winter (Figure 2b). We conclude that our estimate for $F_{\mathcal{N}}$ is reasonable but might contain some contribution from horizontal, advective fluxes.

4.4. Nitrate Drawdown by Primary Production

Following *Codispoti et al.* [2013], we estimated annual new production from nitrate drawdown during the productive period. *Tremblay et al.* [2008] corrected drawdown estimates for changes in salinity, implicitly assuming that any freshwater input was equally depleted in nitrate. For the present data, dilution plays only a small role since the salinity changes by approximately 2.5% between winter and summer. Maximum $\mathcal{N}$ during winter was 10 μM, which means that winter concentrations reach summer concentrations at 70 m. Integrating down to this depth is thus in line with *Codispoti et al.* [2013]. A Redfield C:N ratio [*Redfield et al.*, 1963] of 106:16 (although higher values have been proposed [e.g., *Sambrotto et al.*, 1993], we choose this value for consistency) yields a new production of 31 g C m^{-2}. This coincides with the value *Codispoti et al.* [2013] found for the Nordic Seas and is halfway between their estimates for the Barents Sea (47 g C m^{-2}) and the Eurasian Basin (13 g C m^{-2}), stressing the location of the mooring at the boundary between the shelf and the AO basin.

5. Summary and Perspectives

We present the first annual time series of $\mathcal{N}$ reported from the eastern AO. Based on 1 year of mooring data, we describe the seasonal nitrate cycle together with hydrography, currents, and chl *a* in the surface waters over the shelf slope north of Svalbard. $\mathcal{N}$ followed a seasonal cycle with a maximum in March and a minimum in July–August, linked to abrupt nitrate drawdown by primary producers starting in June, with the timing likely controlled by the presence of ice cover and developing stratification.

In fall and winter 2012, the upward nitrate flux through the nitracline in the AW inflow region was $F_{\mathcal{N}} \approx (2.5 \pm 0.5)$ mmol m^{-2} d^{-1}, constraining the postbloom nitrate supply to the mixed layer. Stratification probably acted as an inhibitor of vertical mixing, and only when stratification became small, mixing was sustained deep enough to erode the vertical $\mathcal{N}$ gradient.

The early date by which the surface nitrate pool was replenished in winter suggests that a lengthening of the productive season has the potential to increase annual new production in the AW inflow area. However, during almost two of the productive summer months, PP was likely not light limited, but nutrient limited, meaning that the potential for increased new production in a scenario with less ice is limited in this location.

The large temporal variability especially during the beginning of the productive season indicates spatial patchiness. This makes it necessary to account for large horizontal gradients in nutrient concentrations, light and ecosystem characteristics, even though the surface waters were clearly dominated by the steadily inflowing modified AW. Caution is thus required when interpreting the temporally isolated vertical profiles usually measured on ship-based campaigns.

Appendix A: Diffusivity Estimates From $F_{\mathcal{N}}$ and HWF Scaling

Estimating the gradient $\partial_z \mathcal{N}$ across 25–45 m from the vertical profiles during the same period Sep/Oct to Dec/Jan, $K = -\frac{F_{\mathcal{N}}}{\partial_z \mathcal{N}} = (5 \pm 1) \cdot 10^{-4}$ m^2 s^{-1} (1 standard deviation from three pairs of flux/gradient estimates). Measurements of eddy diffusivities are generally scattered over orders of magnitude, which makes it difficult to compare this value with observations. To estimate K from stratification and internal wave energy, we use the Henyey-Wright-Flattè (HWF) scaling for the dissipation of turbulent kinetic energy ϵ [*Henyey et al.*, 1986] following *Wijesekera et al.* [1993, equation (8c)]:

$$\epsilon = \frac{1.67}{\pi}\left(bN_0\right)^{-2} f \cosh^{-1}\left(\frac{N}{f}\right) j_*^2 E^2_{\text{meas}} \quad \text{(A1)}$$

with thermocline scale depth $b = 1300$ m, reference buoyancy frequency $N_0 = 3$ cph, and vertical mode scale number $j_* = 3$ and then applying $K = 0.2\epsilon/N^2$ [*Osborn*, 1980]. E_{meas} is estimated as $(\Phi_{uu}+\Phi_{vv})/2$, where $\Phi_{uu,vv}$ are power density spectra of 10 day records of horizontal velocity (u,v) at 35 m depth integrated between f (Coriolis frequency) and 1 cph, neglecting potential energy for simplicity since most of the energy is near inertial. Buoyancy frequency N^2 is estimated as finite difference between 20 and 40 m. Results depend on the exact depth used for horizontal velocities and the time window used to calculate successive spectra but are generally scattered between $K \approx (1-5)\cdot 10^{-4}$ m^2 s^{-1}, which means good agreement with the reasoning that $F_{\mathcal{N}}$ is equal to or smaller than $\Sigma F_{\mathcal{N}}$, especially considering the large uncertainties surrounding dissipation scaling in the ocean.

Acknowledgments

The data used in this study were collected through the project "Long-term variability and trends in the Atlantic Water inflow region" (A-TWAIN), funded by the Arctic Ocean program at the FRAM-High North Research Centre for Climate and the Environment and are accessible by contacting achim@npolar.no. A.R.'s work is supported by the project "CARBON BRIDGE: Bridging marine productivity regimes: How Atlantic advective inflow affects productivity, carbon cycling and export in a melting Arctic Ocean," a Polar Programme (project 226415) funded by the Norwegian Research Council. Vladimir Pavlov provided the processed ADCP data, and Sigrid Øygarden collected the bottle samples. Bottle sample processing was done by Svein Kristiansen (nitrate) and SØ (chl *a*). We thank Ilker Fer and two anonymous reviewers for helpful comments that improved the manuscript and the captain and crew of R/V *Lance* for support in the field.

The Editor thanks two anonymous reviewers for their assistance in evaluating this paper.

References

Aagaard, K., and E. C. Carmack (1994), The Arctic Ocean and climate: A perspective, in *The Polar Oceans and Their Role in Shaping the Global Environment*, edited by O. M. Johannessen, R. D. Muench, and J. E. Overland, pp. 5–20, AGU, Washington, D. C., doi:10.1029/GM085p0005.

Arrigo, K. R., and G. L. van Dijken (2011), Secular trends in Arctic Ocean net primary production, *J. Geophys. Res.*, *116*, C09011, doi:10.1029/2011JC007151.

Arrigo, K. R., G. van Dijken, and S. Pabi (2008), Impact of a shrinking Arctic ice cover on marine primary production, *Geophys. Res. Lett.*, *35*, L19603, doi:10.1029/2008GL035028.

Bourgault, D., C. Hamel, F. Cyr, J.-E. Tremblay, P. S. Galbraith, D. Dumont, and Y. Gratton (2011), Turbulent nitrate fluxes in the Amundsen Gulf during ice-covered conditions, *Geophys. Res. Lett.*, *38*, L15602, doi:10.1029/2011GL047936.

Carmack, E., and D. C. Chapman (2003), Wind-driven shelf/basin exchange on an Arctic shelf: The joint roles of ice cover extent and shelf-break bathymetry, *Geophys. Res. Lett.*, *30*(14), 1778, doi:10.1029/2003GL017526.

Carmack, E., D. Barber, J. Christensen, R. Macdonald, B. Rudels, and E. Sakshaug (2006), Climate variability and physical forcing of the food webs and the carbon budget on panarctic shelves, *Prog. Oceanogr.*, *71*(2–4), 145–181, doi:10.1016/j.pocean.2006.10.005.

Codispoti, L., C. Flagg, V. Kelly, and J. H. Swift (2005), Hydrographic conditions during the 2002 SBI process experiments, *Deep Sea Res., Part II*, *52*(24–26), 3199–3226, doi:10.1016/j.dsr2.2005.10.007.

Codispoti, L., V. Kelly, A. Thessen, P. Matrai, S. Suttles, V. Hill, M. Steele, and B. Light (2013), Synthesis of primary production in the Arctic Ocean: III. Nitrate and phosphate based estimates of net community production, *Prog. Oceanogr.*, *110*, 126–150, doi:10.1016/j.pocean.2012.11.006.

Comiso, J. C. (2012), Large decadal decline of the Arctic multiyear ice cover, *J. Clim.*, *25*(4), 1176–1193, doi:10.1175/JCLI-D-11-00113.1.

Dee, D. P., et al. (2011), The ERA-Interim reanalysis: Configuration and performance of the data assimilation system, *Q. J. R. Meteorol. Soc.*, *137*(656), 553–597, doi:10.1002/qj.828.

Falk-Petersen, S., H. Hop, W. Budgell, E. N. Hegseth, R. Korsnes, T. B. Løyning, J. B. Ørbæk, T. Kawamura, and K. Shirasawa (2000), Physical and ecological processes in the marginal ice zone of the northern Barents Sea during the summer melt period, *J. Mar. Syst.*, *27*, 131–159, doi:10.1016/S0924-7963(00)00064-6.

Henyey, F. S., J. Wright, and S. M. Flatté (1986), Energy and action flow through the internal wave field: An eikonal approach, *J. Geophys. Res.*, *91*(C7), 8487–8495, doi:10.1029/JC091iC07p08487.

Holm-Hansen, O., and B. Riemann (1978), Chlorophyll a determination: Improvements in methodology, *Oikos*, *30*(3), 438–447.

Ivanov, V. V., I. V. Polyakov, I. A. Dmitrenko, E. Hansen, I. A. Repina, S. A. Kirillov, C. Mauritzen, H. Simmons, and L. A. Timokhov (2009), Seasonal variability in Atlantic Water off Spitsbergen, *Deep Sea Res. Part I*, *56*(1), 1–14, doi:10.1016/j.dsr.2008.07.013.

Johnson, K. S., and L. J. Coletti (2002), In situ ultraviolet spectrophotometry for high resolution and long-term monitoring of nitrate, bromide and bisulfide in the ocean, *Deep Sea Res. Part I*, *49*(7), 1291–1305, doi:10.1016/s0967-0637(02)00020-1.

Johnson, K. S., L. J. Coletti, and F. P. Chavez (2006), Diel nitrate cycles observed with in situ sensors predict monthly and annual new production, *Deep Sea Res., Part I*, *53*(3), 561–573, doi:10.1016/j.dsr.2005.12.004.

Osborn, T. R. (1980), Estimates of the local rate of vertical diffusion from dissipation measurements, *J. Phys. Oceanogr.*, *10*(1), 83–89, doi:10.1175/1520-0485(1980)010<0083:EOTLRO>2.0.CO;2.

Redfield, A. C., B. H. Ketchum, and F. A. Richards (1963), The influence of organisms on the composition of sea-water, in *The Sea*, edited by M. N. Hill, pp. 26–77, Academic Press, New York.

Reigstad, M., C. Wexels Riser, P. Wassmann, and T. Ratkova (2008), Vertical export of particulate organic carbon: Attenuation, composition and loss rates in the northern Barents Sea, *Deep Sea Res. Part II*, *55*(20–21), 2308–2319, doi:10.1016/j.dsr2.2008.05.007.

Sakamoto, C. M., K. S. Johnson, and L. J. Coletti (2009), Improved algorithm for the computation of nitrate concentrations in seawater using an in situ ultraviolet spectrophotometer, *Limnol. Oceanogr. Methods*, *7*, 132–143.

Sambrotto, R., G. Savidge, C. Robinson, P. Boyd, T. Takahasahi, D. Karl, C. Langdon, D. Chipman, J. Marra, and L. Codispoti (1993), Net organic carbon production of marine plankton exceeds estimates based on nitrate limitation, *Nature*, *363*, 248–25.

Schauer, U., E. Fahrbach, S. Osterhus, and G. Rohardt (2004), Arctic warming through the Fram Strait: Oceanic heat transport from 3 years of measurements, *J. Geophys. Res.*, *109*, C06026, doi:10.1029/2003JC001823.

Sundfjord, A., I. Fer, Y. Kasajima, and H. Svendsen (2007), Observations of turbulent mixing and hydrography in the marginal ice zone of the Barents Sea, *J. Geophys. Res.*, *112*, C05008, doi:10.1029/2006JC003524.

Torres-Valdés, S., T. Tsubouchi, S. Bacon, A. C. Naveira-Garabato, R. Sanders, F. A. McLaughlin, B. Petrie, G. Kattner, K. Azetsu-Scott, and T. E. Whitledge (2013), Export of nutrients from the Arctic Ocean, *J. Geophys. Res. Oceans*, *118*, 1625–1644, doi:10.1002/jgrc.20063.

Tremblay, J.-E., K. Simpson, J. Martin, L. Miller, Y. Gratton, D. Barber, and N. M. Price (2008), Vertical stability and the annual dynamics of nutrients and chlorophyll fluorescence in the coastal, southeast Beaufort Sea, *J. Geophys. Res.*, *113*, C07S90, doi:10.1029/2007JC004547.

Vancoppenolle, M., L. Bopp, G. Madec, J. Dunne, T. Ilyina, P. R. Halloran, and N. Steiner (2013), Future Arctic Ocean primary productivity from CMIP5 simulations: Uncertain outcome, but consistent mechanisms, *Global Change Biol.*, *27*, 605–619, doi:10.1002/gbc.20055.

Wijesekera, H., L. Padman, T. Dillon, M. Levine, C. Paulson, and R. Pinkel (1993), The application of internal-wave dissipation models to a region of strong mixing, *J. Phys. Oceanogr.*, *23*(2), 269–286, doi:10.1175/1520-0485(1993)023<0269:taoiwd>2.0.co;2.